FINITE ELEMENT MODELLING OF 3D ORTHOGONAL NON–CRIMP WOVEN COMPOSITES

Serra Topal (*)[1, 2-a], Stephen Ogin[3-a], Andrew Crocombe[4-a], Prasad Potluri[5]

[1] Dr., Gazi University, Dept Mechanical Engineering, 06570 Ankara, Turkey, http://w3.gazi.edu.tr/~serra

[2] Visiting Researcher, s.topal@surrey.ac.uk, http://www.surrey.ac.uk/mes/people/visiting_staff/serra_topal.htm

[a] University of Surrey, Dept Mechanical Engineering Sciences, GU2 7XH Guildford, United Kingdom

[3] Professor, s.ogin@surrey.ac.uk, http://www.surrey.ac.uk/mes/people/stephen_ogin/index.htm

[4] Professor, a.crocombe@surrey.ac.uk, http://www.surrey.ac.uk/mes/people/andrew_crocombe/index.htm

[5] Dr., The University of Manchester, School of Materials, M13 9PL United Kingdom,
prasad.potluri@manchester.ac.uk, http://www.manchester.ac.uk/research/prasad.potluri/

ABSTRACT

This paper presents the results of a preliminary finite element analysis conducted for a 3D orthogonal non–crimp woven composite which explicitly, and for the first time, incorporates the through thickness z–binder yarns. A representative volume element (RVE) of the composite has been created to fully model the microstructural arrangement of yarns. The continuously changing material orientations in the z–binder yarns have been incorporated into the finite element software, ABAQUS, by means of input files generated with an open source code program, TEXGEN. The behaviour of the composite has been inspected for the cases of loading in warp and fill (weft) directions. The results show that the fill which is adjacent to the z–binder yarn will fail prior to the warp yarns due to the material's low transverse tensile strength. This phenomenon has been reported in the literature as transverse cracks in fill yarns for the FE case of loading in warp direction. Furthermore, only modest values of tensile stresses have been evaluated on the surfaces of z–crowns, which explain why no initial crack formation could be observed at those regions in experiments. With these results, better understanding of the micromechanical events occurring inside the 3D orthogonal non–crimp woven composite in case of loadings in warp and fill directions has been provided.

Key Words: 3D orthogonal non-crimp woven composites, glass–fibre reinforcement, finite element modelling.

1. INTRODUCTION

A long–standing problem for fibre–reinforced composites is the high risk of delamination since there is only the polymer holding the adjacent plies together. As a solution to this problem, reinforcement in the through–thickness direction has been implemented as a possible solution for more than a decade. This type of reinforcement can be achieved by various techniques, with the most common ones known as three–dimensional (3D) weaving, stitching, and z–pinning [1–3]. Since the last two methods are known to cause piercing, distortions and even fibre breakages in the reinforcement [4], 3D weaving has gained significant interest. Hence, 3D woven composites have become competitive candidates for the applications that require improved delamination and impact resistance; for example, good ballistic impact damage resistance [5] and low–velocity impact damage tolerance [6] have both been reported. The superior damage tolerance is related to the ability of the z–binder yarns to arrest or slow down the growth of delamination cracks under impact loadings [7]. Consequently, 3D woven composites have been considered for utilization in aircraft [8].

In order to realize the potential of 3D textile composites, understanding the microstructure of textile preforms is of significant importance. One of the issues impeding the extensive use of 3D woven composites is the poor understanding of the weaving parameters on the composite properties. Another current impediment to wider application is that their in–plane mechanical properties and failure mechanisms are not well characterised or understood [7].

To address these issues, a number of studies have been published to investigate the mechanical performance of 3D woven fabric composites and progress has been made on modelling their behaviour [9–18]. With regard to finite-element modelling approaches for 3D textile composites, a number of strategies have been adopted. Regarding finite element analysis, Lu *et al* [19] considered the multi-scale finite element analysis of a 2.5D woven composite under on-axis and off-axis tension. They obtained the cross sections of the yarns from measurements made with microscopy. However, these models included only the yarns in a single fibre direction and interlocking yarns between them.

In a different study, Shigang *et al* [20] generated a FE model of a Carbon/Carbon 3D orthogonal woven composite by using two-dimensional images of X-ray micro-computed tomography (μCT) that were captured from the samples. However, the FE models did not include the crimps of the z–yarns; rather they were considered to be straight tows in the third material direction. As a consequence, the results did not include the effect of the crimps on

the textile composite. In the current paper, the complete 3D structure has been modelled, with some simplifications introduced with regard to the actual manufactured fibre architecture.

2. METHODOLOGY

In this study, an approximate representation of the microstructural arrangement of yarns in a real 3D composite is provided by establishing a representative volume element (RVE) of the fabric preform. A RVE constitutes the smallest repeating entity of the structure, and it is assumed that these cells are distributed homogeneously over the entire preform. A RVE identical to that of Bogdanovich [13], Lomov *et al* [21] and Ivanov *et al* [22] has been used in this study and is shown in Figure 1(a). The fibre architecture of the RVE consists of two layers of warp (0˚) and three layers of fill (90˚, also called weft) interlocked with z–binder yarns in the through–thickness direction. Figure 1 (b) shows an optical micrograph of a cross–section of a 3D glass/epoxy orthogonal non–crimp woven composite in the plane of the z–tow [23]. The image depicts the matrix cracks running through the fill yarns and the resin–rich regions between these yarns when the composite has been loaded parallel to the warp yarns. As Fig. 1 (a) shows, the fibre architecture chosen for the FE model is a simplification of the actual fibre architecture of the composite which is more complex. However, the FE model captures the main features of the real fibre architecture.

(a)

(b)
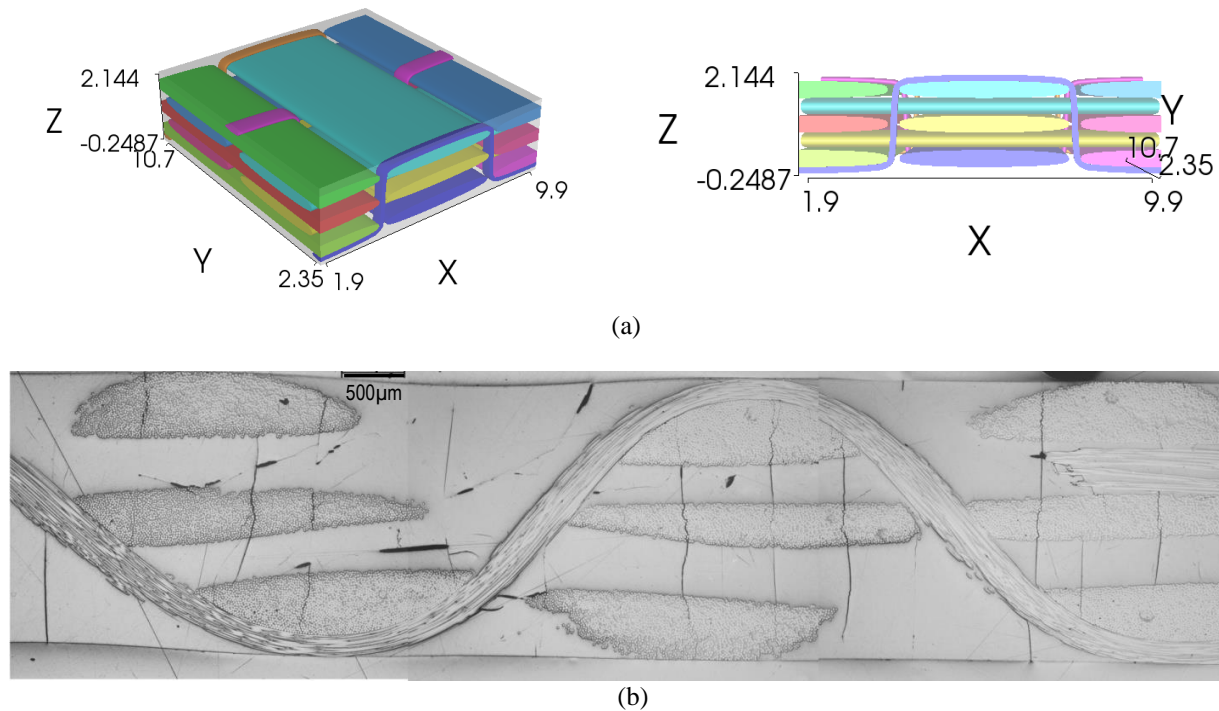
Fig. 1. (a) The RVE of the 3D orthogonal non–crimp woven composite, as seen in the TEXGEN program. (b) Cross–section of a 3D woven composite in the plane of the z–tow showing the actual fibre architecture (Courtesy of Baiocchi [23]).

As the properties of woven composites depend on the geometric pattern of the preform, the properties of the constituent materials and the fibre volume fractions, the FE model yarn dimensions have been constructed using results from X–ray micro-computed tomography (μCT) and microscopy images obtained in recent studies [23, 24]. The cross sections of the fibre yarns have been created as elliptical, with a narrower section for the z–binder yarns. A summary of the principal parameters of the 3D woven composite FE model is provided in Table 1.

Table 1. Summary of principal parameters of the 3D orthogonal non–crimp woven composite model in ABAQUS

Parameter	Finite element model
Composite thickness, mm	2.197
Total fibre volume fraction in composite, %	35.6
Fibre volume contents in a fabric ply: warp/fill/Z, %	32.53/42.87/1.74

The composite thickness value as 2.197 mm is within the value range specified by Lomov *et al* [21], although the fibre volume fraction in this study are lower than the data provided in their paper, since generating all yarns with the same geometrical specifications results in idealized preforms. In the real case, yarns possess different widths and

2

thicknesses, which clearly impacts on the resulting fibre volume fraction in the composite. The fibre volume contents for z–binder yarns are given for the total amount of element volumes in comparison to the total RVE volume. The small value is due to the two halves and a full binder yarn possessing very small cross-sectional size. The set of elastic properties of the isotropic epoxy matrix and orthotropic E–glass fibre material for the resin-impregnated yarns have been taken from the work of Kyriazoglou and Guild [25] and can be seen in Table 2.

Table 2. The elastic material properties of the epoxy matrix and matrix impregnated E–glass fibre reinforcement

Matrix material	Matrix impregnated fibre material		
E = 2 GPa	E_x = 46 GPa	G_{xy} = 5 GPa	ν_{xy} = 0.3
ν = 0.4	E_y = 13 GPa	G_{xz} = 5 GPa	ν_{xz} = 0.3
	E_z = 13 GPa	G_{yz} = 4.6 GPa	ν_{yz} = 0.42

The continuously–changing material orientations for the z–binder yarns have been specified by means of an open source code program called TEXGEN. The commercial FE code for ABAQUS version 6.12 has been used for generating a voxel model with one and a half million eight–noded hexahedral elements [26]. The FE model of the textile material in the form of a dry fibre file as seen in ABAQUS is shown in Figure 2. The arrangement of the fabric yarns and the matrix and the textile preform in the form of voxel file can be seen in Figure 3.

a)   b)
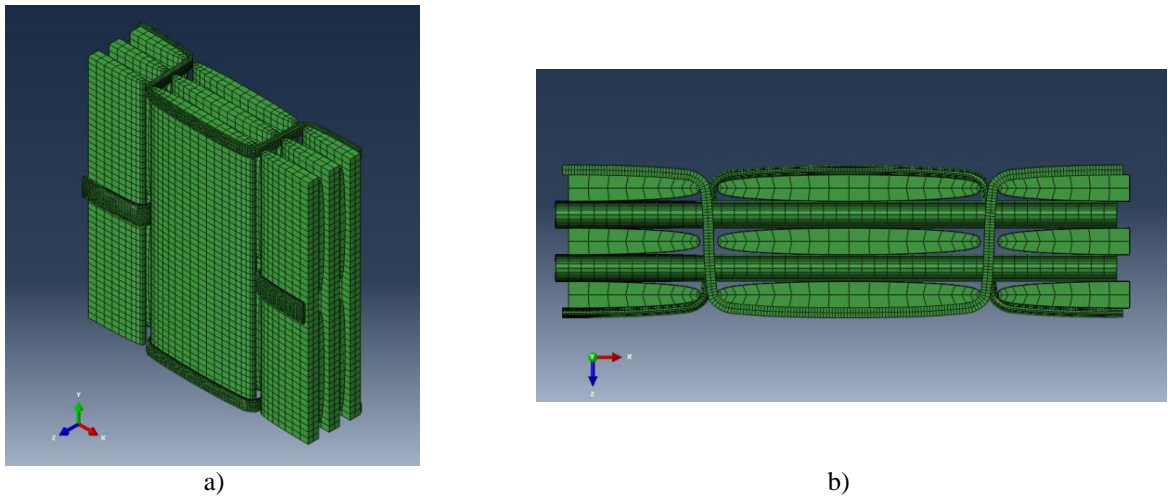
Fig. 2. FE model of the 3D fabric RVE in dry fibre form in ABAQUS for (a) isometric and (b) top views

a)   b)
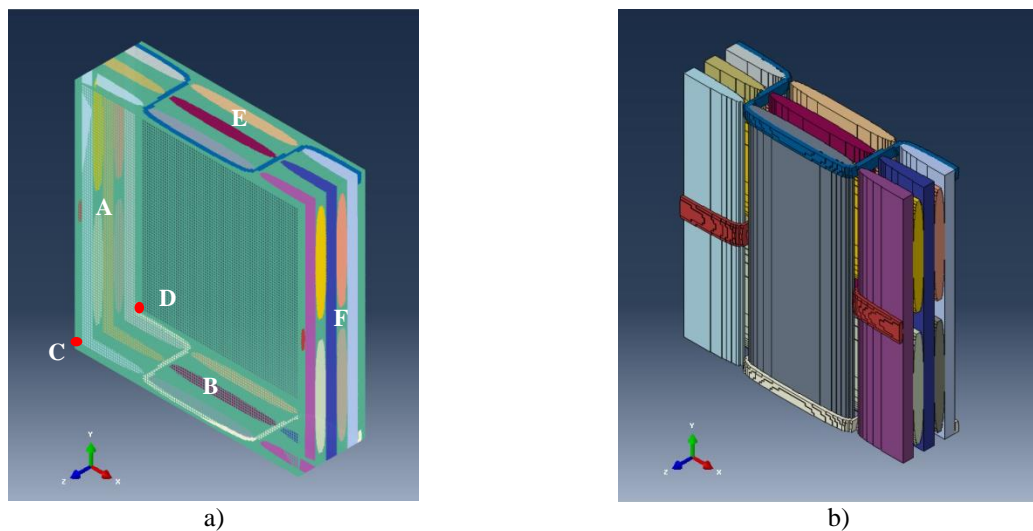
Fig. 3. FE model (a) with and (b) without resin material, and the faces and corners defined for boundary conditions

Displacements normal to two mutually perpendicular faces A and B (Fig. 3 (a)) and displacements in y–direction of the two corners C and D were set to zero while the nodes on face E were constrained to remain planar and the nodes

on face F were given a displacement producing a strain in the warp direction of 1%. The deformation and the stress distributions in the fabric and the matrix material are presented in the next section.

3. NUMERICAL RESULTS

3.1. Loading of the Voxel Model in the Warp Direction

Screenshots showing the magnitude of displacement of the warps, wefts and the z–binder yarns are depicted in Figure 4. Both images display the reference and deformed states together, the initial one as a black wireframe and the latter as a coloured contour plot. These figures show the model is deforming correctly. The distributions of von Mises stresses are shown in Figure 5 for multiple sections in the fabric and the matrix material. As expected, the warp yarns are carrying a higher portion of the load due to their higher modulus in the direction of the loading. As some portion of the load is transferred to the fill yarns, lower stresses are seen in warp yarns at these overlapping sections (yellow regions, Fig. 5(a)). Inspecting the matrix (Fig. 5(b)), shows that high stress concentrations, shown in red, appear at the resin locations between fill yarns, as a result of the very thin resin sections here being subjected to high loads.
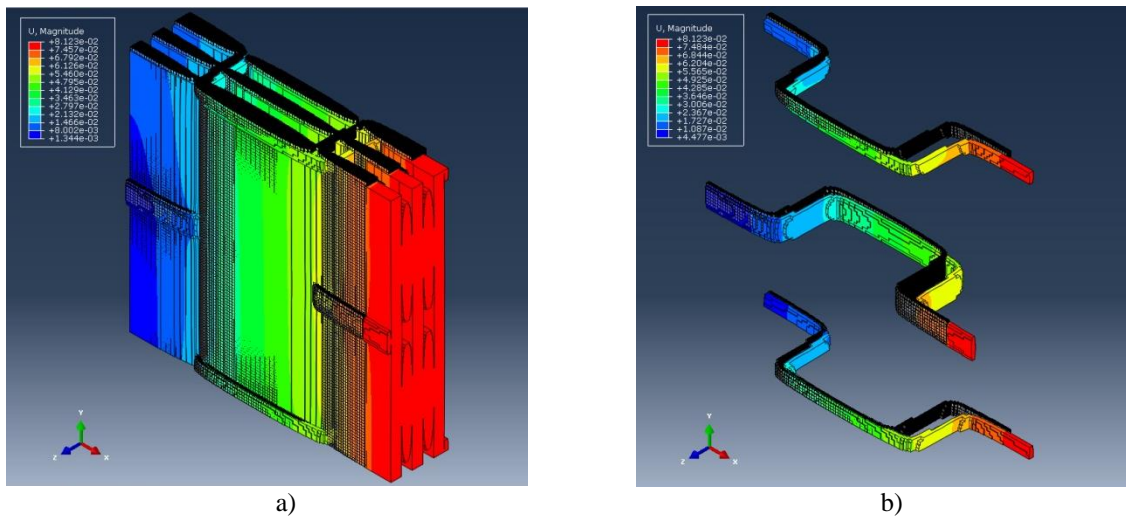
Fig. 4. Deformation of (a) the fabric and (b) the z–binder yarns shown with reference states
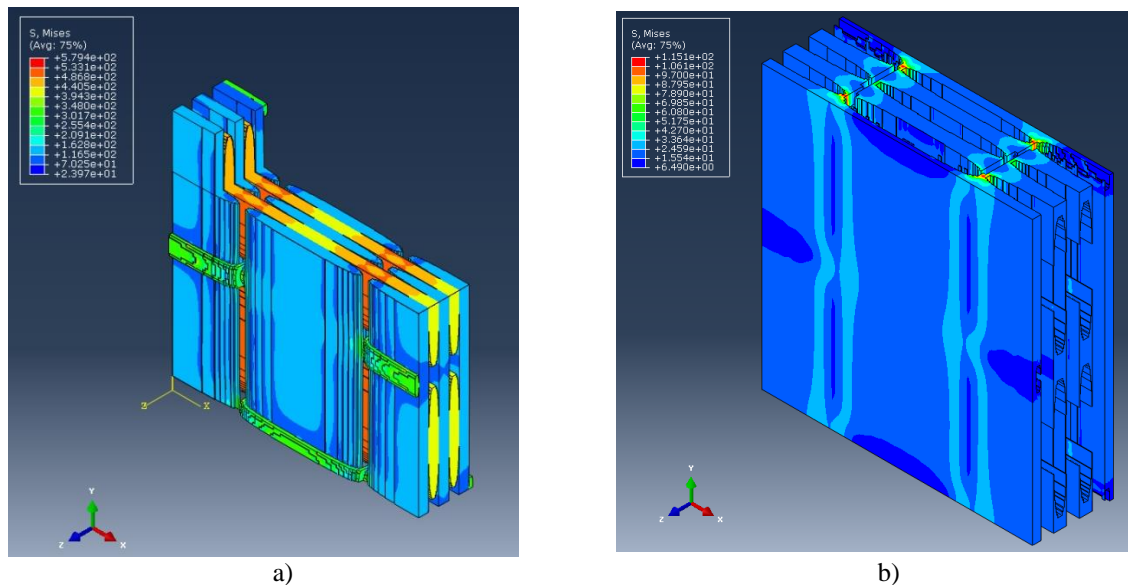
Fig. 5. Von Mises stress distributions for (a) the fibre yarns in a multiple–cut view and (b) for the matrix

For a clearer view of the stresses in the warp yarns, the set of fill yarns in the front row are hidden in Fig. 6 (a). As expected, the x–stresses in the fill yarns are much lower than for the warp yarns while the z–yarns sustain an intermediate level of stress. However, the stresses in the fill yarns exceed the transverse strength of the material. Consequently, matrix cracking is to be expected within the fill yarns, as observed in [22–24].
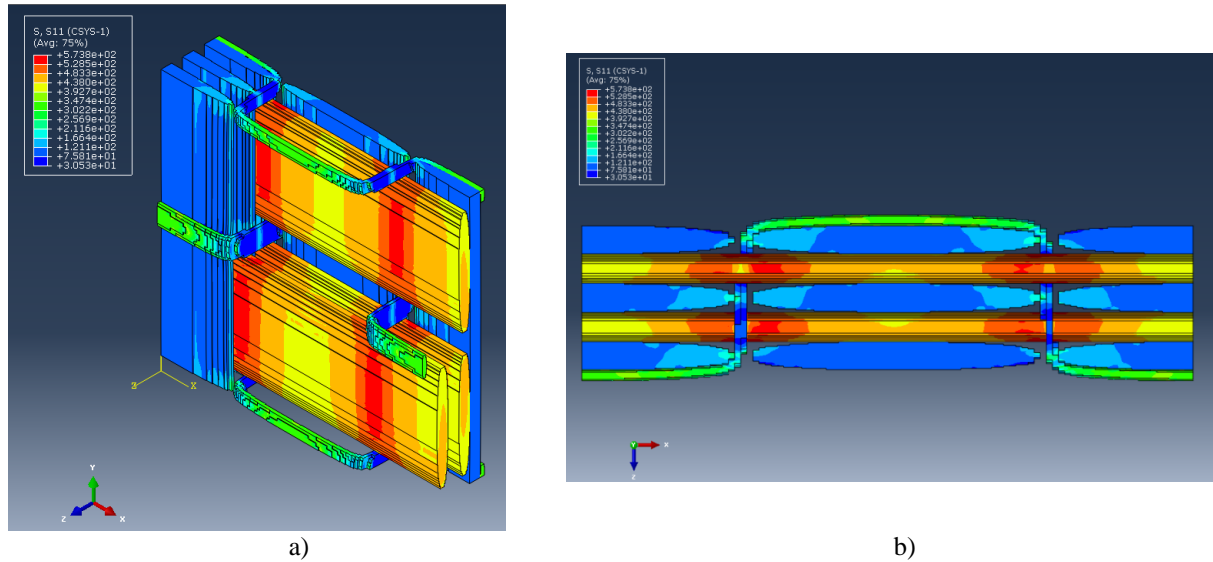
Fig. 6. Stress distributions in the fabric material in +x direction from (a) isometric view and (b) top view
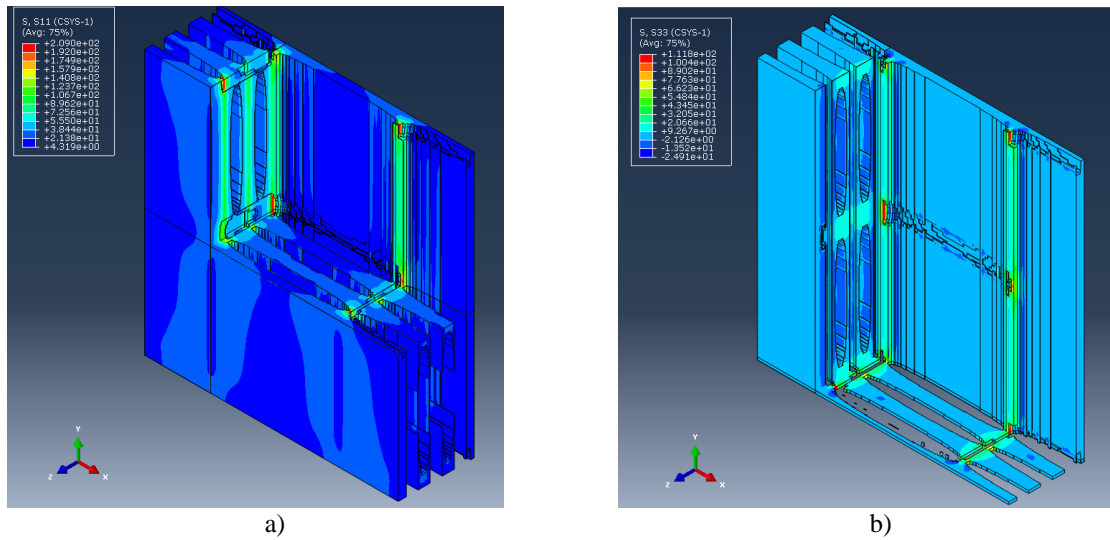
Fig. 7. Stress distributions in the matrix material for (a) +x direction stress and (b) +z direction stress
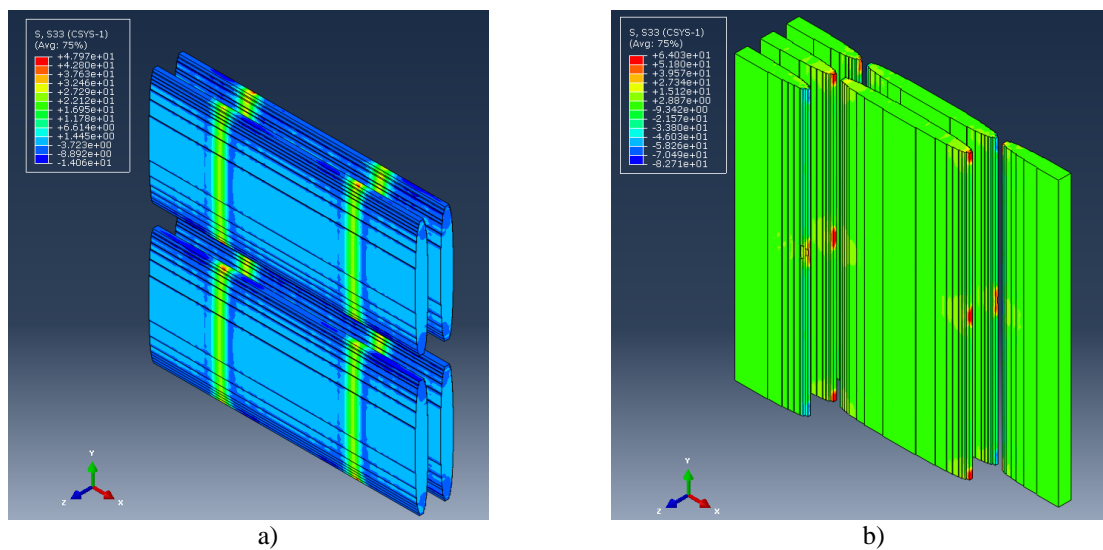
Fig. 8. Stress distributions in +z direction for the (a) warp yarns only and (b) for selected fill yarns

In order to inspect the stress state at different sections in the matrix material, two cut views are provided in Fig. 7, depicting the x–stresses and z–stresses. The epoxy resin is generally under tension due to the elongation in +x

direction and in the resin pockets, running parallel to the weft tows, there is an enhanced stress since the adjacent tows are stiffer drawing in the load (Fig. 7 (a)). These are one of the regions which are prone to transverse cracking during loading in warp direction [22]. As a result of Poisson's contraction in the through–thickness (z–direction), the matrix is generally subjected to compressive stresses in z–direction, but has high tensile stress concentrations where the z–tows loop around the fill yarns (Fig. 7 (b)). From Fig. 8 (a), warp yarns are seen to be under compressive z–stresses except the regions shown in yellow where there are no neighbouring fill yarns. The z-tows also cause compressive and tensile through–thickness stresses concentrations (dark blue and red areas) on the fill yarns at the contact point (Fig. 8 (b)).

The Young's modulus for the 3D model can be evaluated and compared with the experimental value. The total reaction force at the constrained face for a strain of 1% applied in the x-direction was found to be 3.234 kN. Using the cross–sectional area of the RVE, then the Young's modulus in +x direction is approximately 19.9 GPa, which is close to the experimental value of 23.0±2.5 GPa, found for similar 3D woven samples [21]. As a check on this FE derived model, the approximate Reuss and Voigt expressions were applied to the individual layers of the warp and fill yarns (ignoring the z–yarns). This approximate approach results in an overall Young's modulus of about 22 GPa, which is close to the FE model result of 19.9 GPa.

3.2. Loading of the Voxel Model in the Fill Direction

Similar to the loading in the warp direction considered in the previous section, the FE model was also loaded in the fill (or weft) direction. Again, after modification of the boundary conditions and kinematic constraints, a 1% strain has been applied to the FE model in the +y direction. The displacements, von Mises stress distributions in the fibre yarns and in the matrix, as well as the stresses in the yarn sections, are shown in Figures 9 to 12. It can be seen from Fig. 9 (a) that this time the FE model extends in the fill direction, with its elongation constrained at its bottom surface.

a)   b)
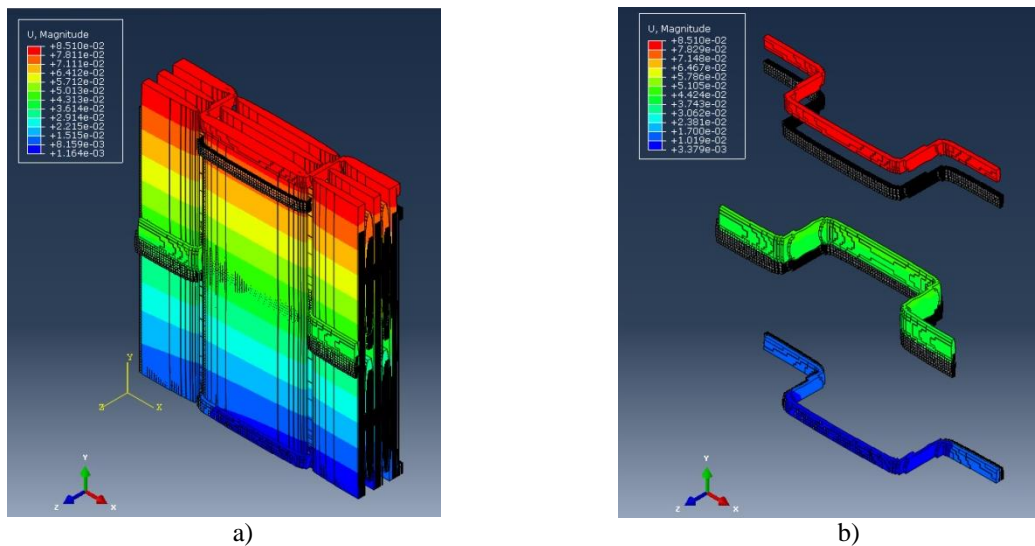
Fig. 9. Deformation of (a) the fibre yarns and (b) the z–tows shown with the reference (undeformed) state

The distribution of von Mises stresses in the fabric (a) and the matrix material (b) can be seen through multiple sections in Fig. 10. While the fill yarns exhibit the highest stresses for this loading direction, the binder yarns have the lower Mises stresses of $6.55 \; 10^1$ to $1.02 \; 10^2$ MPa, since they contribute little to the load carrying of the composite for this direction. This situation is not the same for the case of loading in the warp direction, where z-binder yarn exhibit modest Mises stresses of $2.55–3.45 \; 10^2$ MPa (Fig. 5 (a)).

In Fig. 10 (b), the matrix is seen to be under tension, with the lowest levels of stress occurring around the surfaces of binder yarns (shown in dark blue). On the other hand, the highest stress concentrations in the matrix appear in the areas adjacent to the longitudinal edges of warp yarns, since the warp yarns have a higher transverse modulus than the matrix and draw in the load.
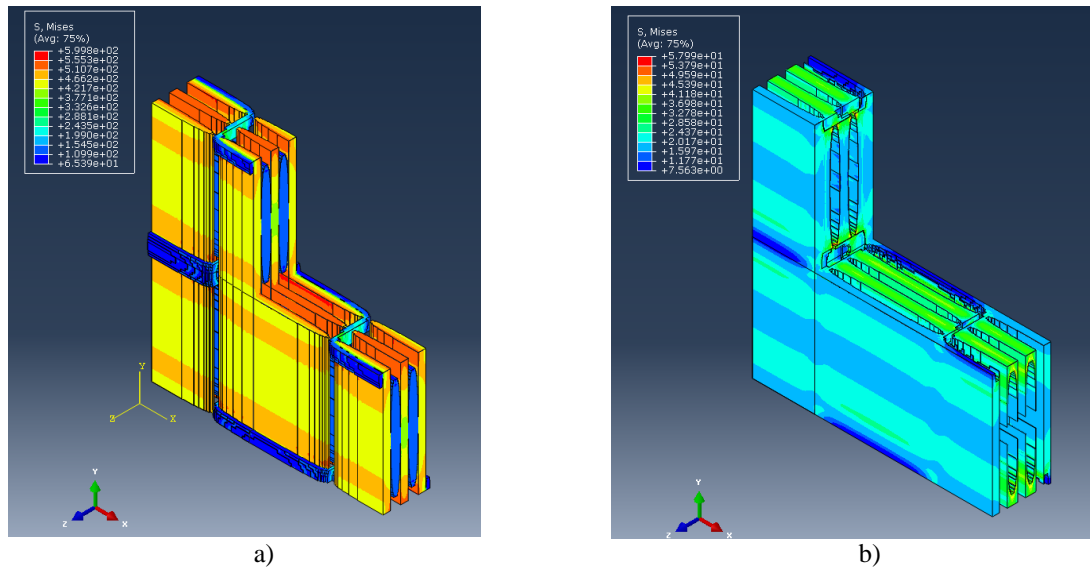
Fig. 10. Von Mises stress distributions in (a) the fibre yarns and (b) the matrix in multiple–cut views
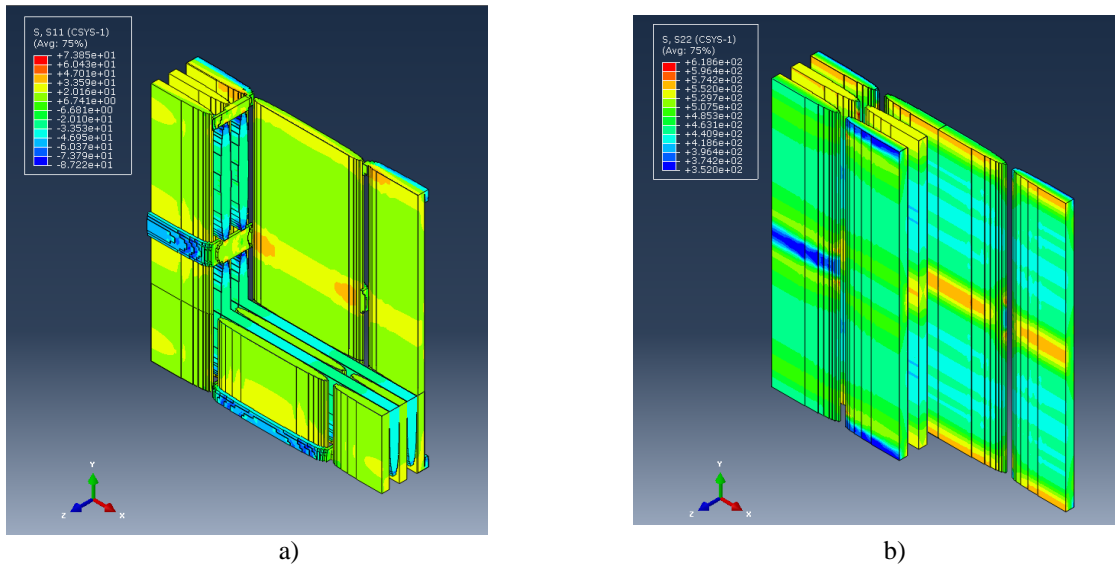
Fig. 11. Stress distributions in (a) +x direction for fabric section and (b) +y direction for the fill yarns only
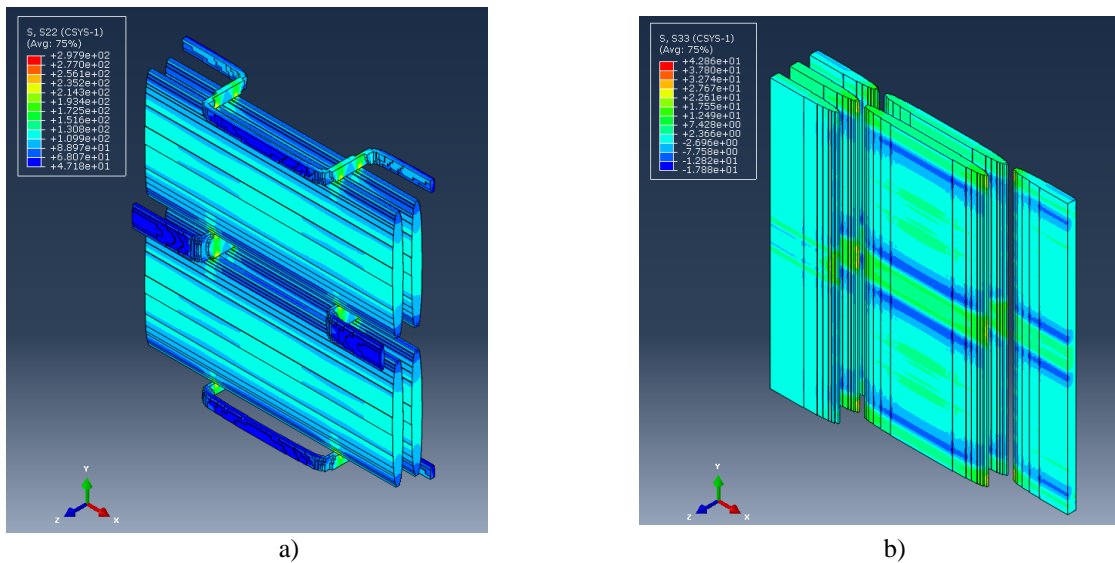
Fig. 12. Stress distributions in (a) +y direction for the warp and z–binder yarns in cut–view and (b) +z direction stresses for selected fill yarns

7

For loading in the +y direction, Poisson's contraction leads to compressive x–stresses in the warp yarns, with the weft yarns put into tension due to the mismatch in Poisson's ratio between the warp and weft yarns (Fig. 11 (a)). As expected, all fill yarns are under tension due to the loading of the composite in that direction. Examination of the Fig. 11 (b) provides clearer influence of the z–tows on the behaviour of the fabric tows (Fig. 11 (b)). It is observed that the regions of the fill under the z–tows are prevented from experiencing higher y–stresses (as shown by the dark blue regions). On the contrary, high tensile stresses are formed in the fill away from the binding yarns (i.e. yellow and orange regions on the front face of the fill yarns).

Regarding the stress distributions in warp and binder yarns in +y direction, the highest stresses are found where the z-tows traverse through-thickness since at these locations the load is shared between the resin-rich regions and the z-tows (Fig. 12 (a)). With regard to the through–thickness (i.e. z–direction stresses) for this direction of loading (parallel to the fill tows) Fig. 12 (b), shows that the contact surfaces of the fill yarns beneath the z–tows have higher tensile z–stresses since local through-thickness contraction is restrained by the z-tows.

The Young's modulus can again be derived, this time for loading in the fill direction. For a 1% strain, the total reaction force at the constrained bottom face was found to be 2.991 kN, suggesting a Young's modulus of 19.2 GPa, which is in reasonable agreement with experimental values of 23.0±2.5 GPa [21].

4. CONCLUSIONS

A preliminary finite element analysis to model the behaviour of 3D orthogonal non–crimp weave reinforced E–glass/epoxy composite has been presented for the case of in–plane tensile loading in warp and fill directions. The model incorporates the through–thickness z–tows which act as binders for the 3D structure. The structure modelled captures the essential features of the actual 3D material, although it is difficult to replicate the precise geometrical features of the actual material. In this preliminary study, the relative magnitudes of stresses for a 1% loading of the composite in the warp or fill directions have been evaluated. In addition, the predicted composite moduli have been found to be in reasonable agreement with experimental values. In subsequent work, it is intended to introduce damage into the model to investigate possible damage mechanisms and the effect on the composite modulus.

REFERENCES

1) Tong L., Mouritz A.P., Bannister M.K. "3D Fibre Reinforced Polymer Composites", Elsevier Science Ltd,. London, United Kingdom, 2002.
2) Dransfield K.A., Baillie C., Mai Y.-W., "Improving the delamination resistance of CFRP by stitching – A Review", *Composites Science and Technology*, 50: 305–17 (1994).
3) Mouritz, A.P., "Review of z–pinned composite laminates", *Composites*, 38 A: 2383–97 (2007).
4) Chou T.W., Ko F.K., "Textile Structual Composites", Volume 3, Composite Materials Series, R.B. Pipes, ed., Elsevier Science Publishers B.V., Amsterdam, Netherlands, 1989.
5) Ko F., Hartman D., "Impact behaviour of 2D and 3D glass-epoxy composites", *SAMPE Journal*, 22: 26–30 (1989).
6) Chou S., Chen H.C., Wu C.C., "BMI resin composites reinforced with 3D carbon-fibre fabrics", *Composite Science and Technology*, 43: 117–28 (1992).
7) Mouritz A.P., Bannister M.K., Falzon P.J., Loeng K.H., "Review of applications for advanced three-dimensional fibre textile composites", *Composites*, 30 A: 1445–61 (1999).
8) Wong R., "Sandwich construction in the Starship", Proceedings of the 37th International SAMPE Symposium, 9–12 March 1992, pp. 186–97.
9) Byun J.-H., Chou T.–W., "Modeling and characterization of textile structural composites: A review", *Journal of Strain Analysis*, 22 (4): 253–62 (1989).
10) Tan P., Tong L., Steven G.P., "Modeling for predicting the mechanical properties of textile composites – A review", *Composites: Part A*, 28: 903–22 (1997).
11) Mouritz A.P., "Tensile fatigue properties of 3D composites with through-thickness reinforcement", *Composites Science and Technology*, 68: 2503–10 (2008).
12) Ansar M., Xinwei W., Chouwei Z., "Modeling strategies of 3D woven composites: A review", *Composite Structures*, 93: 1947–63 (2011).
13) Bogdanovich A.E., "Multi-scale modeling, stress and failure analyses of 3-D woven composites", *Journal of Materials Science*, 41: 6547–90 (2006).
14) Bogdanovich A.E., "Progressive Failure Modeling and Strength Predictions of 3-D Woven Composites", 50th AIAA/ASME/ASCE/AHS/ASC Structures, Structural Dynamics and Materials Conference, 4–7 May 2009, California, pp. 1–20.
15) Lomov S.V., Perie G., Ivanov D.S., Verpoest I., Marsal D., "Modeling three-dimensional fabrics and three-dimensional reinforced composites: Challenges and solutions", *Textile Research Journal*, 81 (1): 28–41 (2011).

16) Whitcomb J.D., "Three-Dimensional Stress Analysis of Plain Weave Composites", *Composite Materials: Fatigue and Fracture*, ASTM STP 1110, T.K. O'Brien, ed., American Society for Testing and Materials, Philadelphia, PA, 471–438 (1991).

17) Woo K., Whitcomb J.D., "Three-Dimensional Failure Analysis of Plain Weave Textile Composites Using a Global/Local Finite Element Method*", Journal of Composite Materials*, 30 (9): 984–1003 (1996).

18) Le Page B.H., Guild F.J., Ogin S.L., Smith P.A., "Finite element simulation of woven fabric composites*", Composites Part A: Applied Science and Manufacturing*, 35: 861–72 (2004).

19) Lu Z., Zhou Y., Yang Z., Liu Q., "Multi-scale finite element analysis of 2.5D woven fabric composites under on-axis and off-axis tension", *Computational Materials Science*, 79: 485–94 (2013).

20) Shigang A., Xiaolei Z., Yiqi M., Yongmao P., Daining F., "Finite element modeling of 3D orthogonal woven C/C composite based on micro-computed tomography experiment", *Applied Composite Materials*, October 2013.

21) Lomov S.V., Bogdanovich A.E., Ivanov D.S., Mungalov D., "A comparative study of tensile properties of non-crimp 3D orthogonal weave and multi-layer plain weave E-glass composites. Part 1: Materials, methods and principal results", *Composites: Part A*, 40: 1134–43 (2009).

22) Ivanov D.S., Lomov S.V., Bogdanovich A.E., Karahan M., Verpoest I., "A comparative study of tensile properties of non-crimp 3D orthogonal weave and multi-layer plain weave E-glass composites. Part 2: Comprehensive experimental results", *Composites: Part A*, 40: 1144–57 (2009).

23) Baiocchi L, October 2013. "Late Fatigue Damage Development in a 3D Woven E-Glass/Epoxy Composite", MSc Thesis, University of Padova, Italy.

24) Kakaratsios Z, August 2010. "Impact Behaviour and Damage Development in Transparent 3-D Woven Composites", MSc Thesis, University of Surrey, United Kingdom.

25) Kyriazoglou C., Guild F.J., "Quantifying the effect of homogeneous and localized damage mechanisms on the damping properties of damaged GFRP and CFRP continuous and woven composite laminates – an FEA approach", *Composites: Part A*, 35: 367–79 (2005).

26) ABAQUS Version 6.12 Documentation Collection. ABAQUS/CAE User's Manual. 2013.